THE JOURNAL OF PHYSICAL CHEMISTRY C

Article

Cite This: J. Phys. Chem. C 2019, 123, 19453−19467

pubs.acs.org/JPCC

DFT + *U* Study of the Adsorption and Dissociation of Water on Clean, Defective, and Oxygen-Covered U_3Si_2{001}, {110}, and {111} Surfaces

Ericmoore Jossou,*[,†] Linu Malakkal,[†] Nelson Y. Dzade,[‡] Antoine Claisse,[§] Barbara Szpunar,[∥] and Jerzy Szpunar*[,†]

[†]Department of Mechanical Engineering, College of Engineering, University of Saskatchewan, 57 Campus Drive, Saskatoon S7N 5A9, Saskatchewan, Canada

[‡]School of Chemistry, Cardiff University, Main Building, Park Place, Cardiff CF10 3AT, U.K.

[§]Westinghouse Electric Sweden AB, SE-721 63 Västerås, Sweden

[∥]Department of Physics and Engineering Physics, College of Art and Science, University of Saskatchewan, 116 Science Place, Saskatoon S7N 5E2, Saskatchewan, Canada

Supporting Information

ABSTRACT: The interfacial interaction of U_3Si_2 with water leads to corrosion of nuclear fuels, which affects various processes in the nuclear fuel cycle. However, the mechanism and molecular-level insights into the early oxidation process of U_3Si_2 surfaces in the presence of water and oxygen are not fully understood. In this work, we present Hubbard-corrected density functional theory (DFT + *U*) calculations of the adsorption behavior of water on the low Miller indices of the pristine and defective surfaces as well as water dissociation and accompanied H_2 formation mechanisms. The adsorption strength decreases in the order U_3Si_2{001} > U_3Si_2{110} > U_3Si_2{111} for both molecular and dissociative H_2O adsorption. Consistent with the superior reactivity, dissociative water adsorption is most stable. We also explored the adsorption of H_2O on the oxygen-covered U_3Si_2 surface and showed that the preadsorbed oxygen could activate the OH bond and speed up the dissociation of H_2O. Generally, we found that during adsorption on the oxygen-covered, defective surface, multiple water molecules are thermodynamically more stable on the surface than the water monomer on the pristine surface. Mixed molecular and dissociative water adsorption modes are also noted to be stable on the {111} surface, whereas fully dissociative water adsorption is most stable on the {110} and {001} surfaces.

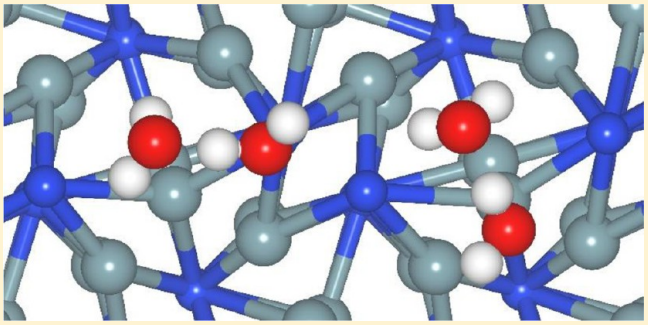

1. INTRODUCTION

There is an increasing interest in the development and use of metallic nuclear fuels such as U_3Si_2 given the enhanced thermophysical properties compared to traditional uranium dioxide fuel (UO_2).[1] However, a key issue to deal with is the ease of oxidation of metallic nuclear fuels in the presence of water, oxygen, or combination of both, which requires the synthesis of U_3Si_2 in controlled environments. A significant number of earlier experimental works have assessed the behavior of U_3Si_2 in corrosion-susceptible environments in comparison to other metallic and UO_2 fuels. Recently, Nelson et al. investigated the behavior of U_3Si_2 following exposure to pressurized H_2O that is typical in light water reactors (LWRs) at temperatures ranging from 300 to 350 °C. Their results showed that both UN and U_3Si_5 rapidly pulverize in less than 50 h at 300 °C, while the behavior of U_3Si_2 was superior but still below the corrosion resistance of UO_2 fuel. It is worth mentioning that the mechanism of pulverization of U_3Si_2 might be due to spallation of UO_2 or due to internal hydriding.[2,3] The formation of $U_3Si_2H_{1.8}$ with volumetric increase has been shown by experiment and density functional theory (DFT) calculations.[4] In this work, we unraveled the detailed mechanism of the early oxidation of U_3Si_2 from an atomistic point of view, which is difficult to realize experimentally. Earlier theoretical works have focused on the bulk properties of U_3Si_2 within the framework of DFT + *U* formalism and molecular dynamics simulations.[4−10] For instance, Middleburgh et al.[4] investigated the defect evolution in U_3Si_2 and also proposed a phase diagram capable of predicting fuel behavior during burnup. Furthermore, Wang et al.[7] studied the electronic, structural, and elastic properties showing detailed bonding characteristics of U_3Si_2 by electron density of states

Received: April 2, 2019
Revised: June 27, 2019
Published: July 11, 2019

DOI: 10.1021/acs.jpcc.9b03076
J. Phys. Chem. C 2019, 123, 19453−19467

(DOS), charge density, and charge density difference analysis which corroborate the work of Remschnig et al.[11] as regards the metallic nature of U_3Si_2.

Surface science provides fundamental insight into the chemistry and physics of corrosion in materials, but such experiments are expensive and require dedicated facilities, especially in the study of an actinide containing compound. Hence, theoretical surface science provides an alternative tool for investigating oxidation mechanisms in nuclear fuel materials. Bo et al.[12] modeled the surface properties of the low-index NpO_2(111), (110), and (100) surfaces as well as the adsorption and dissociation behaviors of water on these surfaces using DFT + U calculations in combination with ab initio atomistic thermodynamic simulations. Their results showed that water dissociation is enhanced by oxygen vacancy, while coverage of the water molecules plays no significant role during molecular adsorption.[13] More recently, Wellington and co-worker investigated the adsorption and dissociation of water on pristine and reduced UO_2 and PuO_2 surfaces using the periodic electrostatic-embedded cluster method and Hubbard-corrected periodic conditions implemented in the DFT-based code. Oxygen vacancies were shown to be easily formed on PuO_2 compared to UO_2, which is due to ease of Pu reduction in comparison to U metal ions. Their results also showed that dissociation is favored over molecular adsorption of water both on defect-free and oxygen deficit surfaces of UO_2 and PuO_2.

Given the success of first-principles DFT + U calculations in the modeling surfaces, we recently studied the adsorption of molecular and dissociated O_2 on stoichiometric U_3Si_2 lower index surfaces.[14] To further our understanding of the underlying mechanism of oxidation, we have considered the synergetic effect of water and oxygen interaction with U_3Si_2 perfect surfaces. However, as real surfaces are never perfect but contain defects due to the method of synthesis or service conditions, in the present work, we have explored the effects of U and Si vacancies on the adsorption mechanisms of water and oxygen on the {001}, {110}, and {111} surfaces of U_3Si_2. Surface vacancies in UN, UO_2, PuO_2, and CeO_2 have been shown in previous studies to affect the oxidation behavior of such surfaces in the presence of oxidizing and hydriding agents.[12,13,15−19] The fundamental aspects of oxygen and water adsorption, including the initial adsorption geometries, adsorption energies, structural parameters, and electronic properties, are presented. Our results reveal a chemical picture of the initial steps involved in the oxidation process of the U_3Si_2 surfaces in the presence of oxygen and water (considering both molecular and dissociative adsorption).

2. COMPUTATIONAL METHODOLOGY

The first-principles calculations were performed within the plane-wave pseudo-potential DFT technique,[20,21] as implemented in the Quantum ESPRESSO code.[22] The exchange−correlation functional potential was described by the generalized gradient approximation (GGA) in the Wu−Cohen (GGA-WC) formulation.[23] All our calculations deployed the norm-conserving Wu−Cohen (WC) pseudopotentials (where these potentials treat $7p^06d^15f^37s^1$ as valence electrons for U and $3s^23p^6$ as valence electrons for Si). Due to the onsite Coulomb repulsion among the localized U 5f electrons, we used the Hubbard (DFT + U) correction to account for the strong correlation effect.[24] We have used an effective U value of 1.5 eV, which has been shown to give an accurate description of the structural parameters and the electronic properties of U_3Si_2.[14]

The Fermi surface effects were treated by the smearing technique of Methfessel−Paxton,[25] using a smearing parameter of 0.02 Ry (0.27 eV). An energy threshold defining self-consistency of the electron density was set to 10^{-8} eV and a β mixing factor of 0.3. The Brillouin zone integration was performed using $7 \times 7 \times 10$ and $5 \times 5 \times 1$ Monkhorst−Pack[22] k-point grids (centered at the Γ point) for the bulk U_3Si_2 and the surface models, respectively. Structural relaxation was carried out to minimize the energy using the conjugate gradient method within the Broyden−Fletcher−Goldfarb−Shanno algorithm,[26] until the magnitude of the residual Hell−Feynman force on each relaxed atom reached 0.01 eV $Å^{-1}$. Visualization and analysis of the structures were performed using the VESTA program.[27,28]

The {001}, {110}, and {111} surfaces were considered for the oxygen and water adsorption calculations as they are the dominant growth facets of U_3Si_2. The different surface structures were created from the fully optimized bulk tetragonal U_3Si_2 structure (Figure 1) to eliminate the presence of fictitious forces during surface relaxation using the METADISE code,[29] which ensures the creation of surfaces with a zero dipole moment perpendicular to the surface plane. A vacuum of 15 Å was introduced to the surface models in the z direction, which is large enough to avoid any spurious interactions between periodic slabs. Bader population analysis was carried out on all adsorbate−substrate systems to quantify any charge transfer between the U_3Si_2 surface and O_2/H_2O species.[30]

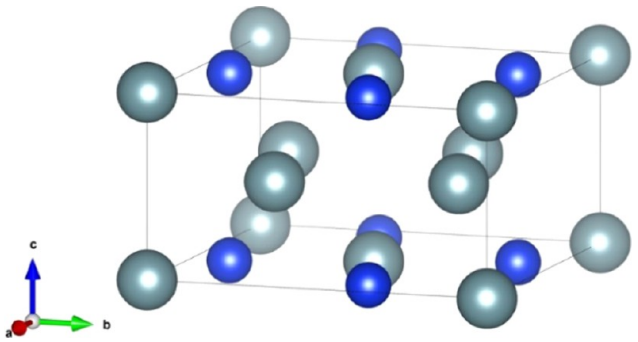

Figure 1. Unit cell of ordered uranium silicide containing two formula units of U_3Si_2 (10 atoms) (color scheme: U = gray and Si = blue).

3. RESULTS AND DISCUSSION

3.1. Defective Surface Models. *3.1.1. Surface Defect Energies and Stability.* Defective surfaces (vacancies) were created by removing one Si/U atom at a time from either the first or second layer (Figure 2) to access their energetics or stability.

The silicon vacancies are denoted as V_{Si}, whereas the two considered uranium vacancy sites are denoted as V_{U1} and V_{U2}, respectively, on the surface. The method of Wellington et al.[19] was employed in the creation of vacancy such that the uranium and silicon atoms removed from the supercell, both from the surface and subsurface layers, are fully coordinated by other quantum mechanically treated atoms and lie close to the center of the supercell to avoid problems that may occur in forming a defect at the edge.[19] The vacancy formation energy was calculated using eq 1

DOI: 10.1021/acs.jpcc.9b03076
J. Phys. Chem. C 2019, 123, 19453−19467

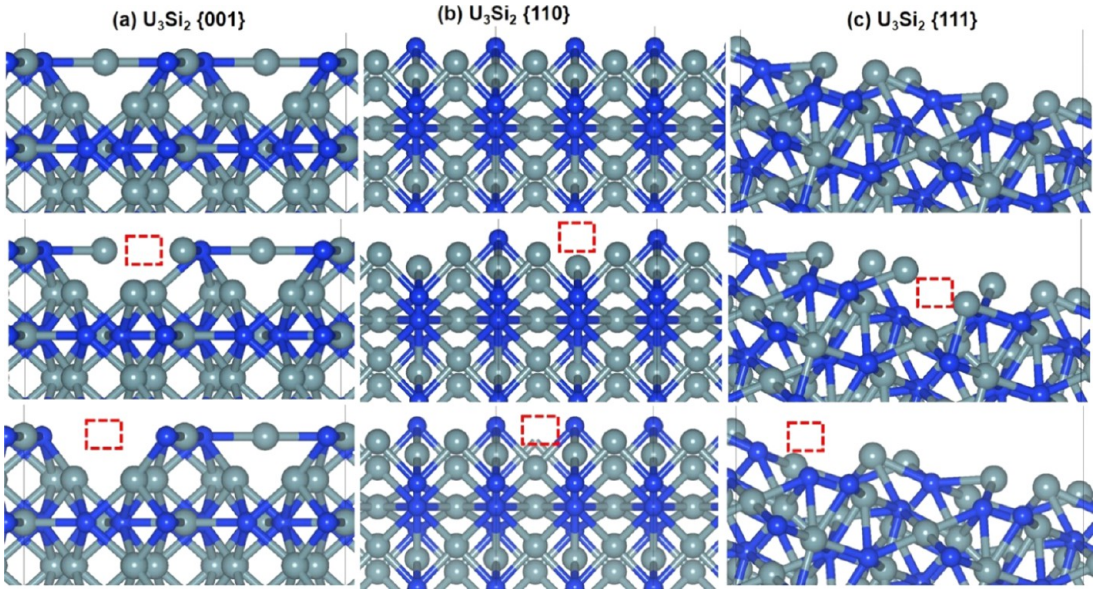

Figure 2. Optimized surface geometry of (a) U_3Si_2{001}, (b) U_3Si_2{110}, and (c) U_3Si_2{111} with Si and U1 surface vacancy represented by a rectangular red box in the second and third rows respectively (color scheme: U = gray and Si = blue).

$$E_{vac} = E_{surface+X_{vac}} - E_{surface} + E_X \quad (1)$$

where $E_{surface+X_{vac}}$ is the energy of the relaxed slab with X = Si or U vacancy, $E_{surface}$ is the energy of the relaxed stoichiometric slab of the same type, and E_X is the reference energy for X = Si and U as the energy per atom in its fundamental face-centered cubic and orthorhombic structure, respectively. Presented in Table 1 are the calculated vacancy formation energies on the {001}, {110}, and {111} U_3Si_2 surfaces. We found higher Si vacancy formation for the {110} surface (2.62 eV) than for the {001} surface (0.16 eV) and {111} surface (1.54 eV), and a similar trend is observed in the subsurface Si vacancies formation. Clearly, Si vacancy on the {110} subsurface (2.62 eV) is close to 2.48 eV, calculated for bulk U_3Si_2 by Andersson et al.[31] This is not surprising, given that the {110} surface has the lowest surface energy and similar neighboring atom coordination. There are two U sites denoted here as U1 and U2 with vacancy defect formation energies of 1.64 and 2.65 eV, respectively, for the bulk. The first and second layer U vacancy energies were calculated as presented in Table 1. Generally, it is easier to form a vacancy in the surface layer compared to the subsurface, which is due to the difference in the nearest neighbor atoms and the coordination numbers.

Table 1. Uranium and Silicon Vacancy Formation Energies (eV) of the {001}, {110}, and {111} Surfaces of U_3Si_2

	first layer			second layer		
surface	V_{Si}	V_{U1}	V_{U2}	V_{Si}	V_{U1}	V_{U2}
{001}	0.16	1.72	1.87	1.74	2.13	2.88
{110}	2.62	3.18	2.41	1.62	2.03	2.61
{111}	1.54	3.81	3.70	2.44	1.46	3.10

The formation of Si and U vacancies resulted in a nonstoichiometric surface, which allows variation in the surface energies as the chemical potential, μ, of Si and U changes. The thermodynamic stability of a given surface, in general, depends on the specific chemical environment. To determine the stability of the surfaces due to vacancies, we calculate the surface energy, γ, as a function of the Si and U chemical potential, respectively. At zero temperature the surface energy of a crystal may be derived from a N-layer slab using eq 2

$$\gamma = \frac{1}{2A}(E_{surf} - NE_{bulk}) \quad (2)$$

In this equation, E_{surf} is the slab energy with all atomic coordinates relaxed unconstrainedly; NE_{bulk} is the energy of an equal number, N of bulk U_3Si_2 atoms; A is the area of the slab surface; and the factor of 2 reflects the fact that there are two surfaces for each slab. Due to the surface vacancy defects, the surface energy depends on the specific thermodynamic conditions, i.e., the reservoir with which the atoms of the compound are exchanged in a structural transition. Therefore, the chemical potential of the constituents enters the surface energy. The most stable surface structure is determined by the minimum of the free energy which at zero temperature is given by eq 3

$$\gamma = \frac{1}{2A}\left[E_{surf} - \sum_i N_i\mu_i\right] \quad (3)$$

In the case of U_3Si_2, eq 3 can be expressed by eq 4 to account for the chemical potential μ of U and Si atoms

$$\gamma = \frac{1}{2A}[E_{surf} - N_U\mu_U - N_{Si}\mu_{Si}] \quad (4)$$

The μ_U and μ_{Si} are bounded by a set of conditions. Assuming U and Si are in thermal equilibrium with the U_3Si_2 crystal, it would imply that

$$\mu_{U_3Si_2} = 3\mu_U + 2\mu_{Si} \quad (5)$$

Furthermore, since there is no precipitation of U and Si on the U_3Si_2 surface, the following conditions must also be fulfilled

$$\mu_{Si}^{surf} \le \mu_{Si}^{bulk},\ \mu_U^{surf} \le \mu_U^{bulk} \quad (6a,b)$$

Also, the heat of formation of bulk U_3Si_2, ΔH_f (eV f.u.$^{-1}$), is defined as

DOI: 10.1021/acs.jpcc.9b03076
J. Phys. Chem. C 2019, 123, 19453−19467

$$\Delta H_f = 3\mu_U^{bulk} + 2\mu_{Si}^{bulk} - \mu_{U_3Si_2}^{bulk} \quad (7)$$

Combining eqs 5, 6a,b, and 7, we obtain a range for possible values of the Si chemical potential

$$\mu_{Si}^{(Si\ bulk)} - \frac{1}{2}\Delta H_{U_3Si_2} < \mu_{Si} < \mu_{Si}^{(Si\ bulk)} \quad (8)$$

Combining eqs 4 and 5, gives the surface energy as a function of μ_{Si}

$$\gamma = \frac{1}{2A}\left[E_{surf} - \frac{1}{3}N_U E_{bulk} + \mu_{Si}\left(\frac{2}{3}N_U - N_{Si}\right)\right] \quad (9)$$

Similar to eq 9, the surface energy can also be expressed as a function μ_U

$$\gamma = \frac{1}{2A}\left[E_{surf} - \frac{1}{2}N_{Si} E_{bulk} + \mu_U\left(\frac{3}{2}N_{Si} - N_U\right)\right] \quad (10)$$

At ambient temperature and pressure, E_{surf} can be taken as the total energy from DFT calculation neglecting contributions from configurational or vibrational entropies. In Figure 2, we show the results of the calculated surface energies of the {001}, {110}, and {111} surfaces of U_3Si_2 as functions of the change in silicon chemical potential μ_{Si}, ranging from Si_4 (−7.46 eV) to that of an isolated Si atom (0 eV), which denotes lower and upper limit of the Si environment, data from NIST database.[32] The lower limit, which is the Si-poor environment, is defined by the decomposition of the silicide into U and Si. Meanwhile, the upper limit is the Si-rich state that corresponds to a situation where the gas phase is so rich in silicon that they condensed on the substrate. In the case of stoichiometric surfaces considered in this work, the surface free energy is independent of μ_{Si} as expected, since the coefficient of eq 6a,ba,b containing μ_{Si} vanishes. For the nonstoichiometric cases, the surface free energy is a linear function of μ_{Si} according to eq 7. It can be seen from Figure 3 that the

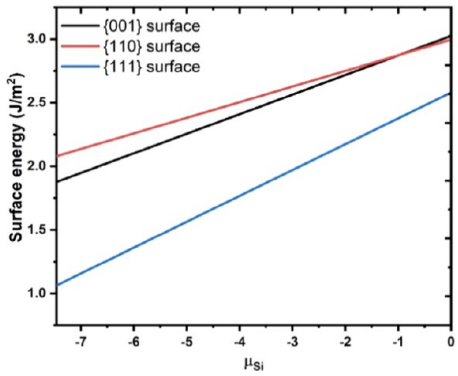

Figure 3. Calculated surface energies of the {001}, {110}, and {111} surfaces of U_3Si_2 as functions of the change in silicon chemical potential μ_{Si}.

equilibrium surface stoichiometry of the U_3Si_2 surfaces can be tuned by changing μ_{Si} through the use of different U_3Si_2 growth (Si vacancy is considered here) and annealing environments. It is clear from the increase in surface energies that the stoichiometric surfaces are found to be more stable than the silicon deficient (silicon vacancy) surfaces. This implies that surface adsorption of an oxidizing adsorbate is more stable on the defective surface in comparison to the stoichiometric surface.

3.2. Adsorption of Water Molecule. The adsorption of the water molecule on the U_3Si_2 surfaces is an important starting step toward understanding its early oxidation mechanisms. The first interest of this study is therefore to determine the lowest-energy adsorption structures and modes of water on the low-index U_3Si_2{001}, {110}, and {111} surfaces, and to characterize the strength of their interaction and the extent of O−H bond activation during the dissociation process. Different H_2O initial adsorption possibilities, including H_w and O_w head-on configurations, have been subjected to geometry optimization until the residual forces on all atoms were ≤0.03 eV $Å^{-1}$. Prior to adsorption, we have calculated the reference energies, bond length, bond angle, and vibrational frequencies of one free H_2O molecule and compared them with earlier theoretical results and available experimental data. The values of the O−H bond and the H−O−H angle of water are determined to be 0.970 Å and 104.5°, respectively, which are in good agreement with the previous experimental and theoretical values.[33,34] The calculated scissoring bend, asymmetric and symmetric stretching vibrational frequencies are calculated to be 1555, 3523, and 3635 cm^{-1}, which agree well with the experimental results (1596, 3652, and 3756 cm^{-1}),[35] thus making our calculation method reliable.

The adsorption energy (E_{ads}), which characterizes the strength of water adsorption has been defined as the mean adsorption energy per molecule of H_2O−U_3Si_2 interaction using eq 11

$$E_{ads} = \frac{1}{n}[E_{surface+n(H_2O)} - (E_{surface} + nE_{H_2O})] \quad (11)$$

where $E_{surface+n(H_2O)}$ is the total energy of the substrate−adsorbate system in the equilibrium state, $E_{surface}$ and nE_{H_2O} are the total energies for the surface and free molecules, respectively, and n is the number of water molecules in the cell. By this definition, a negative value of E_{ads} indicates an exothermic and stable adsorption, whereas a positive value indicates an endothermic and unstable adsorption.

3.2.1. Water Adsorption and Dissociation on Clean U_3Si_2{001}. For the adsorption of molecular water on the U_3Si_2{001} surface, different adsorption sites and configurations were explored to determine the lowest-energy adsorption structures, as presented in Figure 4. The calculated adsorption energies and the optimized interatomic bond distances are summarized in Table 2. The calculated lowest-energy water adsorption structure is presented in Figure 4a, wherein the water molecule adsorbs through the O atom at the U site (U−O = 2.56 Å), releasing an adsorption energy of −3.70 eV. The adsorption of water at the Si site (O−Si = 2.376 Å) released an adsorption energy of −3.11 eV. When the water molecule is adsorbed with the hydrogen atoms pointing toward the surface Si site (Figure 4b), it moved away perpendicularly from the surface during energy minimization until the closest H−Si distance was 3.044 Å. The adsorption energy of this configuration was calculated to be −1.97 eV, while the α(H−O−H) bond angle and O−H bonds are obtained at 102.32° and 0.965/0.967 Å, respectively. Compared to the lowest-energy water adsorption on U_3Si_2{001}, Bo et al. calculated the adsorption energies of −2.07 and −1.27 eV for the lowest-energy adsorption structures of the water monomer on UN(001) and UO_2(110), respectively, which suggest that U_3Si_2{001} is more reactive toward water adsorption than both UN(001) and UO_2(110).[36,37] In all three adsorption modes,

DOI: 10.1021/acs.jpcc.9b03076
J. Phys. Chem. C 2019, 123, 19453−19467

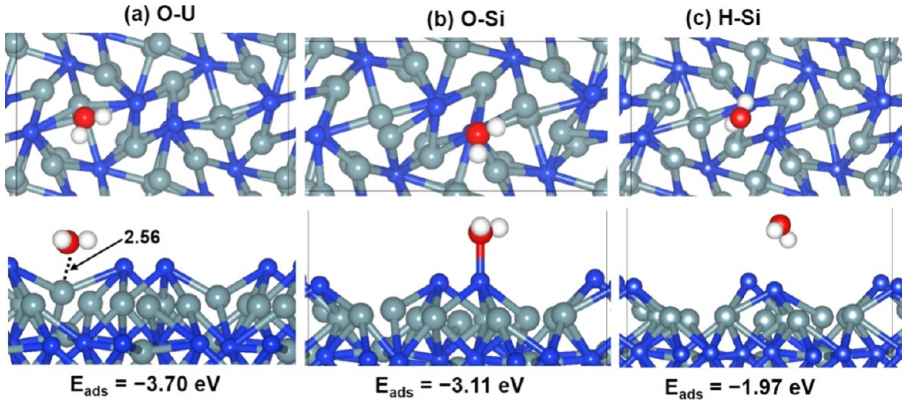

Figure 4. Top and side views of the relaxed adsorption structures of molecular H_2O adsorbed at: (a) O−U, (b) H−Si, and (c) O−Si (color scheme: U = gray, Si = blue, H = white, and O = red).

the O−H bond lengths were slightly elongated and the α(H−O−H) bonds bond angle was larger compared to the gas-phase free H_2O molecule in a vacuum, suggesting that the O−H bonds are activated to some extent when water is adsorbed on U_3Si_2{001}. In the lowest-energy O−U structure (Figure 4a), the two O−H bonds are calculated at 0.975 and 0.996 Å compared to the gas-phase molecule at 0.970 Å and this is consistent with O−H bond stretching vibrational frequencies presented in Table 1, whereas the α(H−O−H) bonds bond angle is obtained at 107.6° compared to the gas-phase value of 104.5°, which is supported by the red and blue shifts in the bending vibrational frequencies as shown in Table 2. The stretched O−H bond lengths are indicative of weaker O−H bonds, resulting from the π-antibonding occupation. The activated O−H bonds suggest that these molecular adsorption states are likely precursors for H_2O dissociation.

Dissociative adsorption of H_2O on the clean U_3Si_2{001} surface is found to be highly exothermic with adsorption energies of −6.81, −5.43, and −3.61 eV, respectively, for the different configurations presented in Figure 5 and Table 2. Consistent with their stronger adsorption, the collective amount of charge transfer gained by the dissociated H_2O species is larger than those of the molecular adsorbed water systems. Due to its metallic nature, the U ions donate more electrons than Si ions during bond formation. The preference for dissociative over molecular adsorption of water can be attributed to the fact that the energy required to break an O−H bond requires less energy compared to the energy released in the formation of the Si−H and U−OH bonds on the U_3Si_2{001} surface. In like manner, on several metals and oxide surfaces, the dissociative state of H_2O is thermodynamically more stable than the molecularly adsorbed state, for example, on Cu and Al_2O_3, because the breaking of an O−H bond is effectively balanced by the formation of a metal−O and another O−H bond with a surface oxygen.[38,39]

3.2.2. Water Adsorption and Dissociation on Clean U_3Si_2{110}. As on the U_3Si_2{001} surface, we have also explored different adsorption configurations of H_2O on the {110} surface, including O adsorbed laterally at U or Si sites or H placed head-on Si sites. The optimized adsorption structures are shown in Figure 6, whereas the energies of adsorption, geometric parameters, and Bader charge transfer analysis are presented in Table 2. The lowest-energy water adsorption configuration at U_3Si_2{110} was calculated to be the O−Si structure (Figure 6a), wherein the water molecule is adsorbed at the Si site through the oxygen atom (O−Si = 2.120 Å), releasing an energy of −2.46 eV. In this structure, we observed elongation of the O−H bond calculated at 0.996 and 0.978 Å, and broadening of the α(H−O−H) bond angle (107.3°). The next stable configuration is the O−U structure (Figure 6b), which released an adsorption energy of −0.60 eV. The interacting O−U distance is calculated at 2.805 Å, and O−H bonds and α(H−O−H) bond angle are calculated at 0.985/1.005 Å and 104.0°, respectively. When the H atoms placed head-on Si (Figure 6c), the adsorption process is found to be endothermic by 0.55 eV and an average O−H bond length is 0.971 Å and there is a preferential Si−O bond formation with an interatomic distance of 1.932 Å after energy minimization. From Bader populations analysis, we found that the adsorption process is characterized by charge transfer from the surface to the water molecule, with the water molecule gaining a charge of $0.15e^-$, $0.16e^-$, and $0.05e^-$ in the O−Si, O−U, and H−Si configurations, respectively. We also observed that the change in the vibrational modes and bond strengths is related to the Bader charge transfer between the surface and the adsorbed water molecule (Table 1).

Compared to the molecular adsorption, dissociative water adsorption is found to have average adsorption energies of −3.24 and −2.27 eV for O_{OH} placed head-on Si and head-on U, respectively. For dissociative adsorption through the H_{OH}, we initially placed an H_{OH} above the Si surface. After optimization, a Si−O bond was formed through the O_{OH} atom, which means that dissociative adsorption through the H_{OH} is unstable. The dissociative adsorption structures are characterized by more electrons being transferred from the surface to the dissociating species as evident by the calculated Bader charges of $0.44e^-$ and $0.17e^-$. The charge transfer from the U_3Si_2 surface to the OH group is a necessary condition for water to bind to the surface, which is consistent with water dissociation on metal surfaces.[40] Furthermore, the above energetics results indicate that the dissociative adsorption of water is notably stronger than the molecular adsorption on the U_3Si_2{110} surface. We also observed the formation of U−H with bond lengths of 2.396 and 2.275 Å in the dissociative configurations, which is required for the H^+ to achieve stability. In comparison to previous work, the U−H distances are 2.30−2.32 Å in α and β-UH_3 configurations.[41] The schematic representations of adsorption structures of dissociated water on the clean U_3Si_2{110} surface are shown in Figure 7.

3.2.3. Water Adsorption and Dissociation on Clean U_3Si_2{111}. The geometries of the lowest-energy adsorption structures obtained on the U_3Si_2{111} surface are shown in

DOI: 10.1021/acs.jpcc.9b03076
J. Phys. Chem. C 2019, 123, 19453−19467

Table 2. Calculated Adsorption Energy (E_{ads}), Relevant Bond Distance (d), Vibrational Frequencies, and Variation of the Total Bader Charge of Molecular (H_2O) and Dissociated (OH + H) Adsorbed on the {001}, {110}, and {111} Surfaces of U_3Si_2

surface	adsorbate	config.	E_{ads} (eV)	d(O−H1) (Å)	d(O−H2) (Å)	d(Si−O) (Å)	d(U−O) (Å)	d(U−H) (Å)	d(Si−H) (Å)	α(HOH) (deg)	ν_b (cm^{-1})	ν_s (cm^{-1})	ν_{as} (cm^{-1})	Δq (e^-)
		H_2O		0.970	0.970					104.490	1555	3523	3635	
{001}	H_2O	O−U	−3.70	0.975	0.996		2.622			107.642	1534	3390	3661	0.08
		O−Si	−3.11	0.994	0.976	2.376	2.562			105.399	1543	3553	3675	0.09
		H−Si	−1.97	0.975	0.977					102.323	1540	3767	3862	0.05
	OH + H	OH−Si: H on adj. U	−6.81	0.983			2.598		1.551					2.13
		OH−Si: H on Si	−5.43	0.971		1.741	2.618		1.501					1.21
		OH−Si: H on U	−3.61	0.965		1.644		2.119						1.17
{110}	H_2O	O−Si	−2.46	0.996	0.978	2.120				107.343	1532	3418	3673	0.15
		O−U	−0.60	0.985	1.005					104.041	1600	3326	3590	0.16
		H−Si	0.55	0.971	0.970					103.232	1601	3425	3571	0.05
	OH + H	OH−Si: H on U	−3.24	0.979		1.676		2.396	1.583					0.44
		OH−U: H on Si	−2.27	0.974			2.200		1.510					0.17
{111}	H_2O	O−U	−1.40	0.977	0.995		2.548			105.454	1543	3432	3690	0.19
		H−Si	−0.20	0.957	0.977					99.181	1575	3677	3948	0.05
		O−Si	1.02	0.977	0.982					102.205	1622	3584	3691	0.01
	OH + H	OH−U: H on Si	−3.30	0.971			2.194		1.697					2.18
		OH−Si: H on U	−1.21	0.969		1.702		2.181						0.34

J. Phys. Chem. C 2019, 123, 19453−19467 DOI: 10.1021/acs.jpcc.9b03076

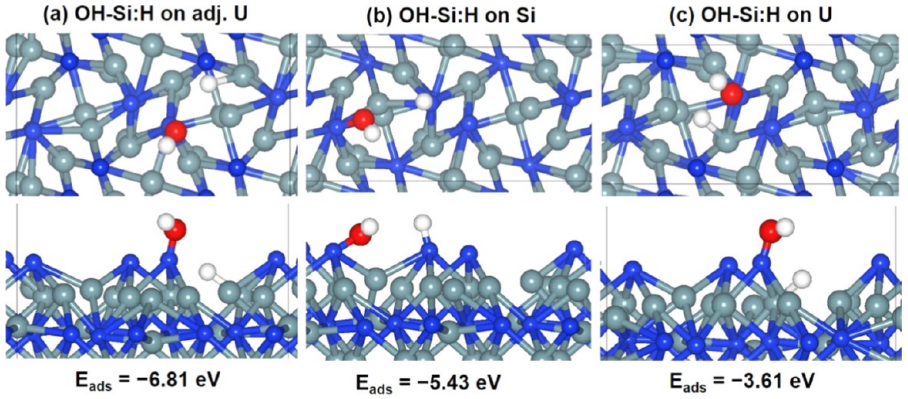

Figure 5. Top and side views of the relaxed adsorption structures of dissociated water configuration with (a) OH−Si: H on adj. U, (b) OH−Si: H on Si, and (c) OH−Si: H on U, on the $U_3Si_2\{001\}$-Si terminated surface (color scheme: U = gray, Si = blue, H = white, and O = red).

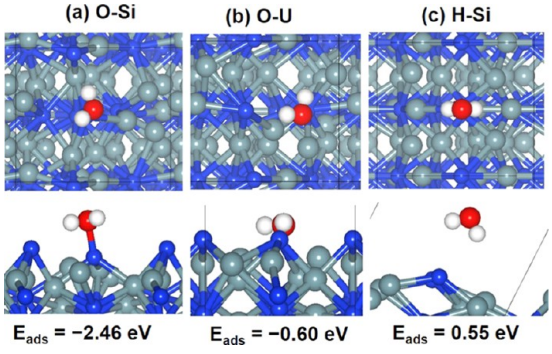

Figure 6. Top and side views of the relaxed adsorption structures of molecular oxygen adsorbed at (a) O−Si, (b) O−U, and (c) H−Si on the $U_3Si_2\{110\}$ surface (color scheme: U = gray, Si = blue, H = white, and O = red).

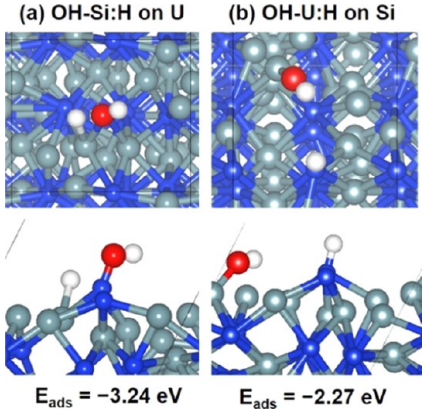

Figure 7. Top and side views of the relaxed adsorption structures of dissociated H_2O at (a) OH−Si: H on U and (b) OH−U: H on Si on the $U_3Si_2\{110\}$ surface (color scheme: U = gray, Si = blue, H = white, and O = red).

Figure 8a−c. Compared to the {001} and {110} surfaces, the water molecules are adsorbed least strongly on the {111} surface. The lowest-energy adsorption structure on the $U_3Si_2\{111\}$ surface is calculated to be the O−U configuration (Figure 8a), which released an adsorption energy of −1.40 eV. In this structure, the water molecule binds via the O atom lying laterally above the U atom at an O−U distance of 2.548 Å, with the α(H−O−H) bond angle that slightly increased to 105.5° compared to the gas-phase value of 104.5°. When the H_2O molecule is adsorbed with the H atoms pointing toward the surface Si atoms (Figure 8b), an adsorption energy of −0.20 eV was released. The closest distance between H and Si/U sites is calculated to be 2.632/2.942 Å ruling out the formation of silane and uranium hydrides. The O−H bond lengths are elongated within the range of 0.977−0.995 Å while the α(HOH) bond angle increased slightly by 0.964° as presented in Table 2. The adsorption of H_2O through O_w is unstable with an endothermic energy of 1.20 eV and tends to move further away from Si after optimization as shown in Figure 8c.

For dissociative adsorption of water on $U_3Si_2\{111\}$, the OH radical and one H atom are placed on the surface with two different adsorption modes as shown in Figure 9a,b. In Figure 9a, the OH^- forms a bond with a surface U atom while the H atom bonded to a neighboring Si atom. The formed U−O, Si−O, and Si−H bond lengths are 2.655, 1.722, and 1.610 Å, respectively. The calculated adsorption energy for this configuration is −0.76 eV, whereas the adsorption of O_{OH} on U leads to the formation of U−O (2.194 Å) and Si−H (1.697 Å) bonds after optimization requiring an energy of −3.30 eV. The larger adsorption energies suggest a preference for dissociative water adsorption over molecular adsorption on the $U_3Si_2\{111\}$ surface, which is consistent with previous studies of uranium-bearing systems.[37,42,43]

3.3. Effects of Surface Coverage, O-Covered, and Surface Vacancy on Adsorption of Water. *3.3.1. Water Adsorption at Higher Coverage.* The effect of coverage on the adsorption properties of water on the U_3Si_2 surfaces was investigated by adsorbing up to four water molecules in a molecular, mixed, and partially dissociative modes. The optimized structures of the most stable adsorption modes are shown in Figure 10, whereas the adsorption energies are reported in Table 3. We found no clear trends in the adsorption energies with an increasing number of water molecules on the U_3Si_2 surfaces. At the {001} surface, the adsorption energies of one, two, three, and four water molecules representing a coverage of 0.25, 0.50, 0.75, and 1.00 monolayers (ML) are −3.70, −2.83, −3.02, and −3.10 eV, respectively. At the {110} surface, the adsorption energy increased from −2.46 eV for one water molecule to −3.23, −3.06, and −2.58 eV for two, three, and four water molecules, respectively. A decrease in the adsorption energy is observed at the {111} surface with an increasing number of water molecules; −3.30 for one water molecule compared to

DOI: 10.1021/acs.jpcc.9b03076
J. Phys. Chem. C 2019, 123, 19453−19467

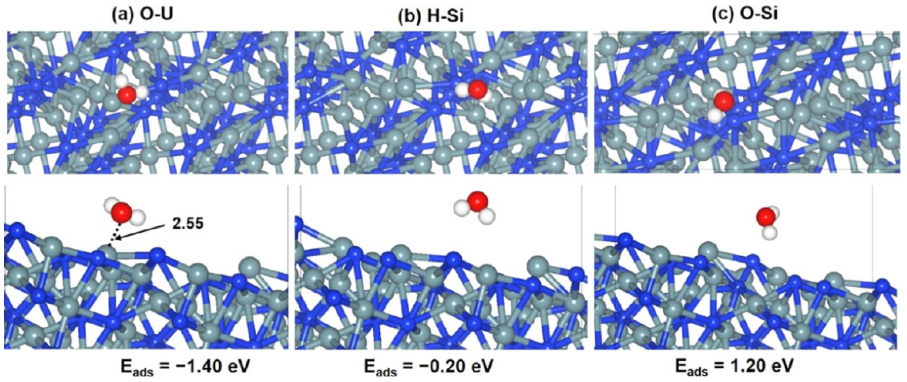

Figure 8. Top and side views of the relaxed adsorption structures of molecular H_2O adsorbed at (a) the O−U site, (b) the H−Si site, and (c) the O−Si site on the U_3Si_2{111} surface (color scheme: U = gray, Si = blue, H = white, and O = red).

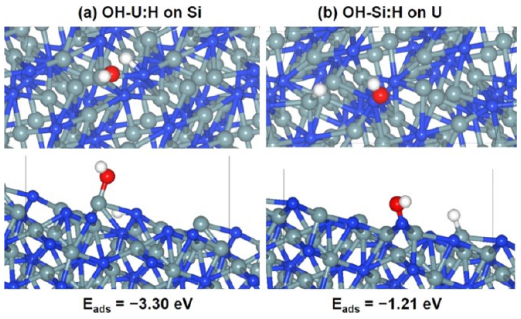

Figure 9. Top and side views of the relaxed adsorption structures dissociated water configuration with (a) O−U: H and (b) O−Si: H, on the U_3Si_2{111}-Si terminated surface (color scheme: U = gray, Si = blue, H = white, and O = red).

−1.42, −2.01, and −2.53 eV for the two, three, and four water molecules, respectively.

Apart from the molecularly adsorbed water molecules, we have also explored mixed adsorption modes, wherein some of the water molecules are dissociated and some remained molecularly adsorbed, and investigated the case of fully dissociated modes in which all of the water molecules are dissociated at full coverage. The optimized structures of the most stable adsorption states are shown in Figure 10, and the adsorption energies are reported in Table 3. The mixed adsorption modes of molecular and dissociative water results in the formation different oxides, hydroxides, and oxygen molecules on the U_3Si_2 surface depending on the ratio of dissociative to molecularly adsorbed water as shown in Figure 10 for the most stable adsorption energies. The remaining structures are given in the Supporting Information (Figures S1−S3). For instance, on the {001} surface, in the case of 75/25 mix adsorption, the oxygen molecule was formed with a bond length of 0.99 Å directly on the surface Si with a bond distance of 1.70 Å typical of SiO_2 formation. The strongest and most stable adsorption modes at the {001} surface are predicted for 3D + 1M, which released an adsorption energy of −4.12 eV, compared to the 4D structures on the {110} and {111} surfaces, which released adsorption energies of −3.68 and −3.45 eV, respectively. Even though U_3Si_2 is a metallic fuel, it is important to draw a comparison between the silicide and urania, which is the standard fuel for LWRs. Hence, it is interesting to note that studies by Bo et al.[37] on UO_2 and

Table 3. Adsorption Energies (eV) per Water Molecule, Mixed Molecular and Dissociated Water on U_3Si_2 Surfaces[a]

adsorbate	{001}	{110}	{111}
1M	−3.70	−2.46	−3.30
2M	−2.83	−3.23	−1.42
3M	−3.02	−3.06	−2.01
4M	−3.10	−2.58	−2.53
1D + 3M	−3.25	−2.68	−2.69
2D + 2M	−3.26	−2.69	−2.65
3D + 1M	−4.12	−2.72	−2.48
4D	−3.54	−3.68	−3.45

[a]Where M = H_2O and D = OH + H.

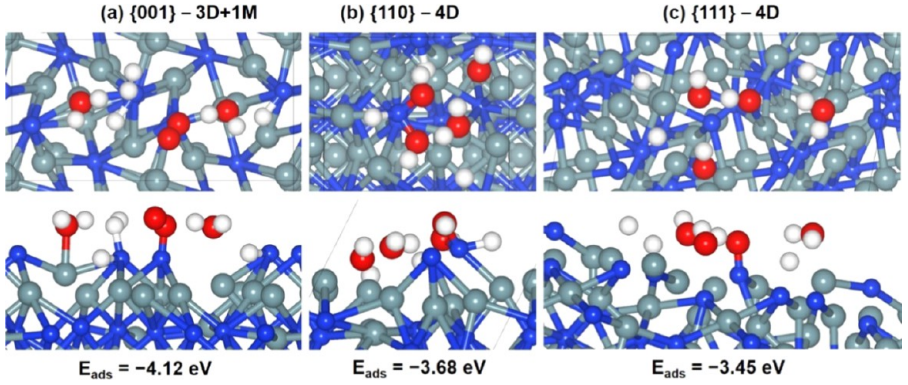

Figure 10. Top and side view of the relaxed adsorption structures of mixed (dissociative to molecular) 3:1 adsorption of H_2O on (a) {001} and fully dissociative adsorption of H_2O on (b) the {110} and (c) {111} U_3Si_2 surface (color scheme: U = gray, Si = blue, H= white, and O = red).

DOI: 10.1021/acs.jpcc.9b03076
J. Phys. Chem. C 2019, 123, 19453−19467

Table 4. Selected Interatomic Distances (Å) for Molecular and Dissociative Water on the U_3Si_2{001}, {110}, and {111} Surfaces at Coverages from 0.5 to 1.0 Monolayers (ML)

bond type	{001} 0.5−1.0 ML (Å)	{110} 0.5−1.0 ML (Å)	{111} 0.5−1.0 ML (Å)
Si−O	1.70	N/A	N/A
Si−H	1.50−1.71	1.57−1.60	N/A
Si−OH	1.66−1.68	1.67−1.68	1.62−1.70
Si−H_2O	1.89−2.11	2.02−2.06	N/A
U−O	2.13	N/A	N/A
U−H	2.17−2.34	2.34−2.45	2.16−2.35
U−OH	N/A	2.31−2.78	2.48−2.71
U−H_2O	2.51−2.67	2.35−2.65	2.64−2.69

recent work by Tegner et al.[44] predicted the mixed 50/50 molecular/dissociative adsorption modes as the most stable adsorption configurations. The differences in the results can be attributed to differences in the crystallographic arrangement of the two systems and their electronic structures, UO_2 is a semiconductor with an experimental band gap of 2.1 eV,[45,46] whereas U_3Si_2 is metallic. Note, however, that the energy difference between the fully dissociative case and the fully molecular case is −0.44, −1.10, and −0.92 eV on the {001}, {110}, and {111} surfaces, respectively. The increase in adsorption energies in the dissociative configuration is due to the formation of stronger intramolecular hydrogen bonds on the crowded surfaces compared to the purely molecular mode.

We also carried out a detailed analysis of the bond lengths for molecular and dissociative adsorption of multiple water molecules on the surfaces as shown in Table 4. We observed a shorter hydrogen bond length for the Si−H compared to U−H on the U_3Si_2{001}, {110}, and {111} surfaces, which suggest stronger hydrogen bonding in Si−H when it is formed on the surface. There is also strong adsorption of molecular H_2O on the surface forming U−H_2O and Si−H_2O complexes with the exception of the {111} surface where the formation of Si−H_2O is not observed.

3.3.2. Water Adsorption and Dissociation on O-Covered U_3Si_2{100}, {110} and {111} Surfaces. Preadsorbed oxygen atoms play an important role in the activation of the O−H bond and further increase the rate of surface oxidation due to rapid water dissociation.[47,48] Hence, it is important to investigate the adsorption behavior of H_2O on oxygen-covered U_3Si_2{001}, {110}, and {111} surfaces. Prior to investigating the adsorption of H_2O on oxygen-covered U_3Si_2{001}, {110}, and {111} surfaces, we have systematically characterized the adsorption of atomic oxygen on different U_3Si_2 surfaces to elucidate their surface oxide formation. In our previous study,[14] we have provided comprehensive information regarding the mechanism of oxide layer formation on the U_3Si_2 surface by adsorbed O_2 molecule. The adsorption of atomic O is found to be energetically more favorable at U sites than Si sites on the {001}, {110}, and {111} U_3Si_2 surfaces (Table S4 and Figure S5). The adsorption energies at the U and Si sites were calculated to be −2.44 and −0.67 eV on the {001} surface, −2.71 and −0.77 eV on the {110} surface, and −2.85 and −0.81 eV on the {111} surface. Similar results were predicted for molecular O_2 at the different U_3Si_2 surfaces, which implies that the formation of UO_2 on pristine U_3Si_2 is favored over SiO_2.[14]

For the adsorption of water on the O-covered U_3Si_2 surfaces, various coadsorption structures were explored with the water adsorbed at the neighbor or distant sites from the preadsorbed O atoms. The coadsorption energies between the H_2O and O on the U_3Si_2 surface is calculated as follows

$$E_{\text{co-ads}} = E_{\text{surface}+(H_2O+O)} - (E_{\text{surface}} + E_{H_2O} + 1/2E_{O_2})$$

where E_{H_2O}, E_{O_2}, E_{surface}, and $E_{\text{surface}+(H_2O+O)}$ are the total energy for the free molecule of water, molecular oxygen, the clean U_3Si_2 surface, and the coadsorbed $(H_2O + O) + U_3Si_2$ surface systems, respectively. In most cases at the {001} surface, we found that the water molecule coadsorbed with oxygen dissociate to form OH ions due to the attractive force between the hydrogen atoms and preadsorbed O atoms. The most favorable coadsorption mode on the {001} surface is predicted for the configuration in which the water molecule is adsorbed at the U site near the O atom that is preadsorbed at the Si site. Due to the strong attractive force between the two adsorbates, the H_2O molecule spontaneously dissociate to form two hydroxyl species, releasing an adsorption energy of −5.47 eV (Table 5), which is consistent with water dissociation on oxygen-covered metal surfaces.[34,49] The U−OH and Si−OH interaction bond lengths are calculated to be 2.339 and 1.641 Å, respectively. Consistent with the strong adsorption, the two OH species draws a combined charge of $1.95e^-$ from the interacting surface species. When the water molecule remained molecularly adsorbed at a Si site near a preadsorbed O atom (Figure 11b), an adsorption energy of −3.54 eV is released.

We have also investigated the adsorption and dissociation of water on the U_3Si_2{110} surface in the presence of preadsorbed atomic oxygen. Three coadsorption modes have been explored with the H_2O and O coadsorbed at the neighboring surface U and U bridge sites. The optimized adsorption geometries are shown in Figure 12a−c, while the coadsorption energies and the relevant optimized geometric parameters are summarized in Table 5. When water is adsorbed with the O_w head-on Si and the preadsorbed O atom at the nearest neighbor U−U bridge, the coadsorption energy is −7.41 eV, which is more negative than the sum of the separate adsorption energies (−3.23 eV), suggesting a strong interaction evident by the stretching of the OH bonds and significant transfer of electrons $(1.21e^-)$ from Si to the water molecule. It is clear that the oxygen atom has a stronger affinity for the uranium forming a U−O−U complex with a bond angle of 97.65°. Hence, the water molecule preferred to bond with the surface Si atom rather than deprotonate to form hydroxyl ions as was observed on iron sulfide surfaces.[34] When water is coadsorbed with the O_w head-on a neighboring U site, the coadsorption energy is calculated to be −4.13 eV, which is also more negative than the sum of the separate adsorption energies (−3.31 eV), suggesting that the oxygen atom promotes the dissociation of water due to deprotonation resulting in the formation of silane (Si−H), uranium oxide (U−O), and

DOI: 10.1021/acs.jpcc.9b03076
J. Phys. Chem. C 2019, 123, 19453−19467

Table 5. Calculated Adsorption Energy (E_{ads}) and Relevant Bond Distances for H_2O Coadsorbed with Atomic Oxygen on $U_3Si_2\{001\}$, $U_3Si_2\{110\}$, and $U_3Si_2\{111\}$ Surfaces

surface	adsorbate	config.	E_{ads} (eV)	$d(O_w–H1)$ (Å)	$d(O_w–H2)$ (Å)	$d(O–H2)$ (Å)	$d(Si–O)$ (Å)	$d(Si–OH)$ (Å)	$d(U–O)$ (Å)	$d(U–OH)$ (Å)	$a(HOH)$ (deg)	Δq (e^-)
{001}	H_2O + O	H_w–U: O on U	−5.47	0.977		1.026		1.641		2.339		1.95
		O_w–Si: O on Si	−3.54	0.970	0.988		1.729		2.525		106.760	1.83
		O_w–Si: O on U	−3.49	0.975		0.953		1.680		2.525		1.79
		O_w–U: O on Si	−2.87	0.973		1.099	1.675					1.75
{110}	H_2O + O	O_w–U: O on U bridge	−7.41	0.975	0.975		2.763		2.268		105.523	1.21
		O_w–Si: O on U	−4.13	0.982					2.236			0.92
		H_w–Si: O on U	−3.67	0.978		1.154				1.80		
{111}	H_2O + O	O_w–Si: O on U	−1.39	0.979		1.006		1.710		2.145		1.67
		O_w–U: O on Si	−0.81	0.977	0.974		1.695		2.567		109.975	1.87
		H_w–Si: O on U	−0.27	0.974					2.021			

hydroxyl (O–H) species (Figure 12b). In this case, where H_w is placed on the Si atom, we observed a repulsion between H and Si while the nearest O atom forms a bond with one of the H_w leading to the formation of hydroxyl ions as shown in Figure 12c releasing an energy of −2.67 eV.

The most favorable coadsorbed configuration of the (H_2O + O)/U_3Si_2 system on the {111} surface is found to be the structure with the water molecule adsorbed on Si while one of the hydrogen atoms pointing toward the preadsorbed O atom on the top-U site (Figure 13a) releasing an energy of −1.39 eV, which is more negative than the sum of the separate adsorption energies of 0.39 eV. This is indicative of attraction between the two species on the $U_3Si_2\{111\}$ surface for this configuration. This accounts for the dissociation of the water molecule leading to the formation of two Si–OH and U–OH. Although in the adsorption of the O atom on the Si site (Figure 13b) leads to the O atom, preferentially forming a trihedral network with U and Si atoms, this is facilitated by drawing electrons from a metal surface that is easy compared to a Si atom while there is stretching of the OH bonds (0.977 and 0.974 Å) with the O_w forming bond with the surface U atom.

3.3.3. Water Adsorption on Defective (Nonstoichiometric) Surfaces. Considering that real surfaces are never perfect under reaction conditions and chemical processes often occur at defect sites, we have also investigated water adsorption at the defective surfaces containing one Si or U vacancies at the {001}, {110}, and {111} surfaces. The optimized structure of defective U_3Si_2 with H_2O is shown in Figure 14 and the calculated adsorption energies and optimized geometry parameters are listed in Table 6. At the defective {001}, {110}, and {111} surfaces containing one Si vacancy site (Si-1), the adsorption energies of the water monomer in the molecular state is calculated to be −7.52, −3.18, and −7.0 eV, respectively. In {001} and {110} adsorption structures, there is a complete dissociation of the water molecule which is consistent with the chemisorbed nature of water[16] while the OH bonds on the {111} surface stretch to 1.245 and 0.980 Å, respectively, suggesting the instability of the water molecule on the nonstoichiometric surface. The computed bond distance of U–O (2.163–2.321 Å) and Si–O (1.536–1.892 Å) suggest the formation of UO_2 and SiO_2.

At the surfaces containing one U vacancy site (U-1), the dissociative adsorption of H_2O on the defective $U_{3-x}Si_2\{110\}$ is found to be highly exothermic (E_{ads} = −5.84 eV), which suggests that the defective $U_{3-x}Si_2\{001\}$ favors dissociative H_2O adsorption rather than molecular adsorption, similar to the findings on the defective $U_{3-x}Si_2\{001\}$ and {111} surfaces. Bader population analysis reveals that a significant amount of charge (~1.32e^-) was transferred to dissociated water species from the interacting surface species. This is not surprising since vacancies result in the formation of dangling bonds (reactive sites) due to the availability of electrons for transfer to water molecules on the surface.

3.4. Electronic Structure and Bonding Mechanism. Fundamental understanding of the nature of interactions between the H_2O molecule and the U_3Si_2 surfaces and any adsorption-induced changes in the electronic structures of U_3Si_2 were gained through projected density of states (PDOS) analysis (Figure 15). The empty (filled) electronic states near the Fermi level can accept (donate) more electrons to enhance the reduction (oxidation) reactions. We observed various degrees of shifts in the PDOS, indicative of a change in the

DOI: 10.1021/acs.jpcc.9b03076
J. Phys. Chem. C 2019, 123, 19453–19467

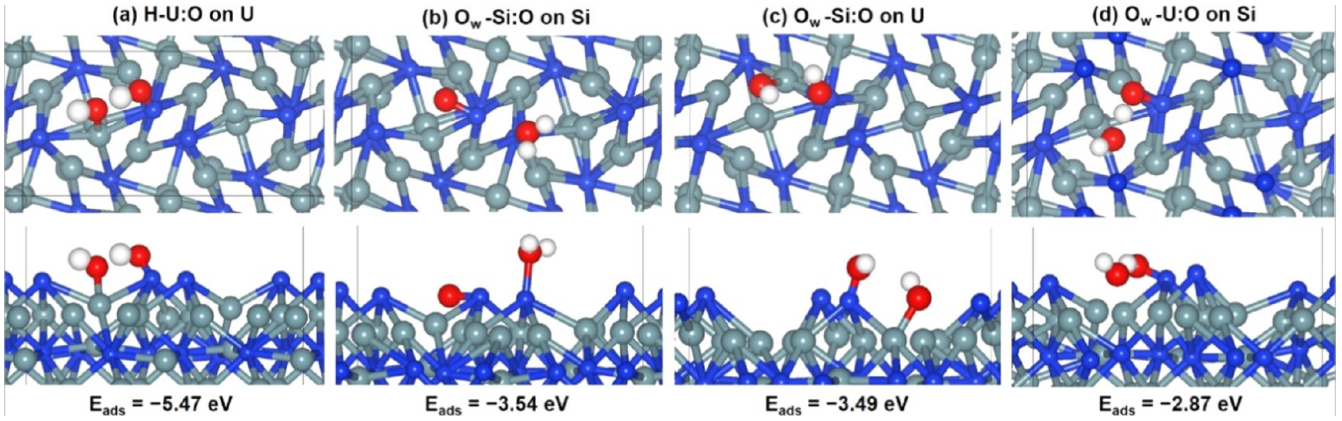

Figure 11. Top and side views of the relaxed adsorption structures of molecular H_2O (a) H−U: O on U, (b) O_w−Si: O on Si, (c) O_w−Si: O on U, and (d) O_w−U: O on Si U_3Si_2{001} surface (color scheme: U = gray, Si = blue, H = white, and O = red).

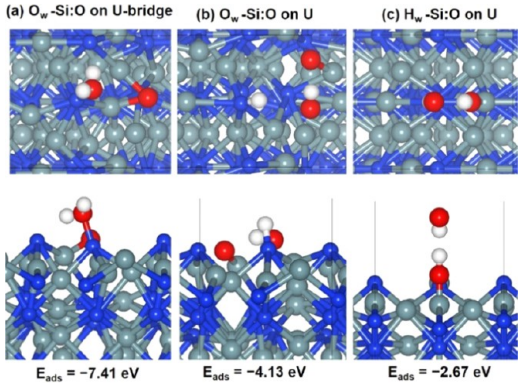

Figure 12. Top and side views of the relaxed adsorption structures of molecular H_2O (a) O_w−Si: O on the U bridge, (b) O_w−Si: O on U, and (c) H_w−Si: O on U on the U_3Si_2{110} surface (color scheme: U = gray, Si = blue, H = white, and O = red).

electronic structure due to electron transfer from U and Si ions to the water molecules leading to OH bond elongation; a step before deprotonation of the water molecule. The charge gained by the H_2O molecule in different adsorption complexes is calculated to be in the range of 0.05−0.11e^- at the water−U_3Si_2{001} surface, 0.04−0.05e^- at the water−U_3Si_2{111} surface, and 0.15−0.25e^- at the water−U_3Si_2{110} surface (Table 3).

There is a possibility of surface oxide formation as shown by the U−O bond lengths of 2.620 and 2.555 Å and Si−O bond length of 2.120 Å on the {001}, {111}, and {110} surfaces, respectively. This suggests that water−U_3Si_2 oxidation would proceed by any of the following chemical reactions[50,51]

$$U_3Si_2 + 10H_2O \rightarrow U_3O_8 + 2SiO + 10H_2,\ \Delta H = -6.695\ \text{eV}$$

$$U_3Si_2 + 12H_2O \rightarrow U_3O_8 + 2SiO_2 + 12H_2,\ \Delta H = -9.815\ \text{eV}$$

$$U_3Si_2 + 8H_2O \rightarrow 3UO_2 + 2SiO + 8H_2,\ \Delta H = -8.105\ \text{eV}$$

$$U_3Si_2 + 10H_2O \rightarrow 3UO_2 + 2SiO_2 + 10H_2,\ \Delta H = -11.222\ \text{eV}$$

The reaction energy of the different possible reaction pathways is found to be highly exothermic, which suggest that they are thermodynamically favorable and feasible reactions.

We further analyzed the PDOS of the isolated water molecule in the adsorbed state at the various surfaces and compared to the gas-phase molecule (Figure 16). The DOS for the gas-phase H_2O molecule is shown in Figure 16a where the

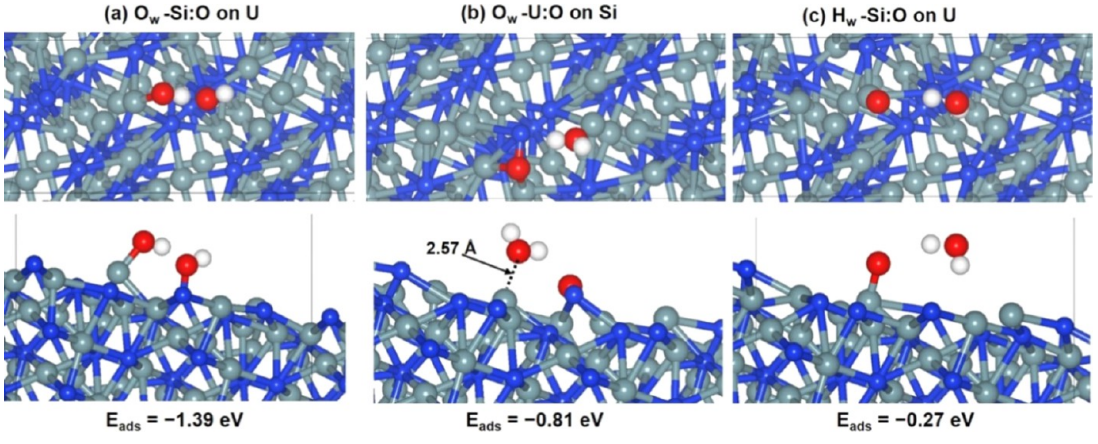

Figure 13. Top and side views of the relaxed adsorption structures of molecular H_2O (a) O_w−U: O and (b) O_w−Si: O on the U_3Si_2{111} surface (color scheme: U = gray, Si = blue, H = white, and O = red).

DOI: 10.1021/acs.jpcc.9b03076
J. Phys. Chem. C 2019, 123, 19453−19467

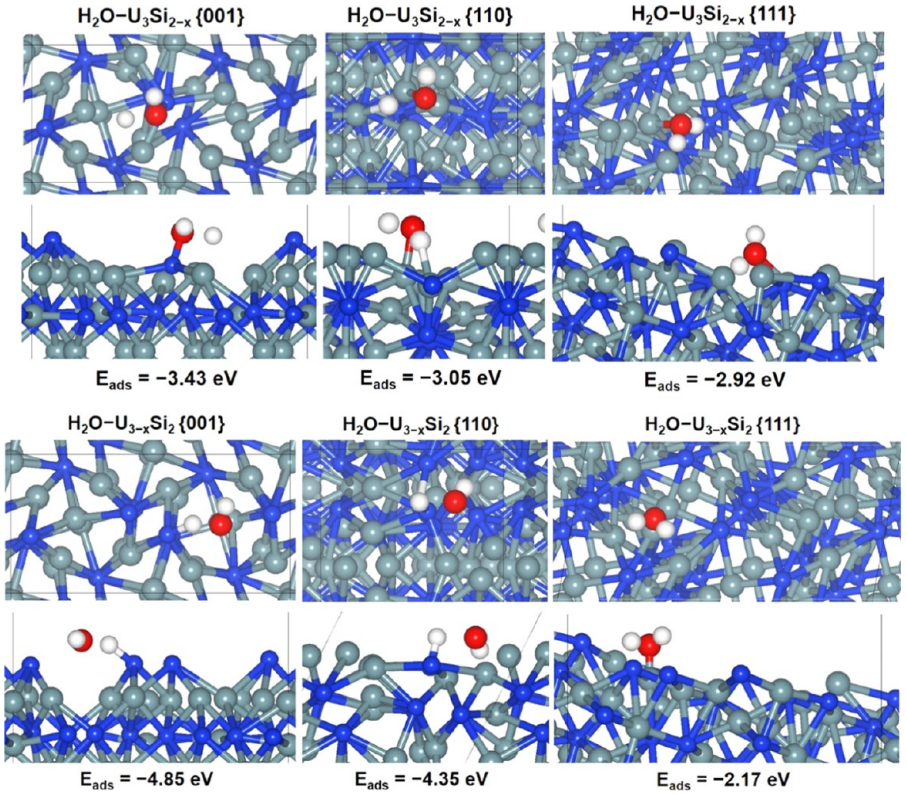

Figure 14. Top and side views of the relaxed adsorption structures of Si and U vacancy-assisted molecular H_2O adsorption (a) H_2O−U_3Si_{2-x} {001}, (b) H_2O−U_3Si_{2-x} {110}, (c) H_2O−U_3Si_{2-x} {111}, (d) H_2O−$U_{3-x}Si_2${001}, (e) H_2O−$U_{3-x}Si_2${110}, and (f) H_2O−$U_{3-x}Si_2${111} surface (color scheme: U = gray, Si = blue, H = white, and O = red).

Table 6. Adsorption Energies (eV) of the Water Molecule on Nonstoichiometric U_3Si_2{001}, {110}, and {111} Surfaces

adsorption site	{001}	{110}	{111}
Si vacancy	−3.43	−3.18	−2.92
U1 vacancy	−4.85	−4.35	−2.17
U2 vacancy	−5.84	−4.22	−3.54

molecular orbitals (MOs) are labeled as 2a1, 1b2, 3a1, and 1b1, respectively, while those for the lowest-energy adsorption configurations at the water−U_3Si_2{001}, {110}, and {111} interfaces are shown in Figure 16b−d, respectively. Due to the strong water−U_3Si_2 hybridization, electron transfer from the interacting surface U f-states, we observed a shift or disappearance of the 3a1 and 1b1 MOs around the Fermi level of water adsorbed at the {001} and {111} surfaces. At the water−U_3Si_2{110} interface, we observe a splitting of the 1b1 MO, coupled with a shift toward lower energy levels (Figure 16d), which signifies stabilization of the water molecule via physisorption. The reactivity of the surface is influenced largely by the ease of electron transfer between the surface and the adsorbate. Previous, work by Li et al. showed that the electronic states of the valence band of the surface play a key role during the surface−adsorbate interaction due to the hybridization energy between the bonding and antibonding adsorbate states and the metal valence-bands.[52]

As the preadsorbed oxygen species enhance the O−H bond activation to dissociate, a necessary step for the formation of surface oxides, we have also characterized the electronic structures of the O-covered U_3Si_2 surfaces and showed that the U atoms to which atomic oxygen is bound become more positive ($1.12e^-$, $1.20e^-$, and $1.61e^-$ on the {001}, {110}, and {111} surfaces, respectively) compared to the clean surface U charge of $+0.98e^-$ {001}, $0.96e^-$ {110}, and $1.01e^-$ {111}, which, from the qU^{4+}/qU^{6+} ratio, is enough to suggest that they have been oxidized from U^{4+} to U^{6+} (see Table S4 and Figure S5, for full details of O−U_3Si_2 in terms of bond lengths and charge transfer). We further investigated the nature of the interaction of the bonding between surface U and atomic oxygen by analyzing the projected density of states (PDOS) of the interacting surface U f-states and O p-state, as shown in Figure 17. We observed strong hybridization between the interacting U f-states and O p-state, which is due to the charge transfer from surface U ions into the adsorbed oxygen π orbital, in good agreement with previous studies of oxygen adsorption on metal surfaces[53]

The work function gives a picture of the nature of such electronic interactions; hence, we have calculated the work function of the clean and adsorbate containing U_3Si_2 surfaces to characterize the level of difficulty for an electron transferring from the surface to the vacuum. The work function is the minimum energy needed to remove an electron from the bulk of a material through a surface to a point outside the material and can be written as

$$\Phi = V_{\text{vacuum}} - E_{\text{Fermi}} \tag{12}$$

The potential in the vacuum region (V_{vacuum}) and the Fermi energy (E_{Fermi}) were derived from the same calculation. In practice, this is the energy required at 0 K to remove an electron from the Fermi level of the material to the vacuum potential. We determined the work function of the clean surface and further probed the effect of oxygen on the

DOI: 10.1021/acs.jpcc.9b03076
J. Phys. Chem. C 2019, 123, 19453−19467

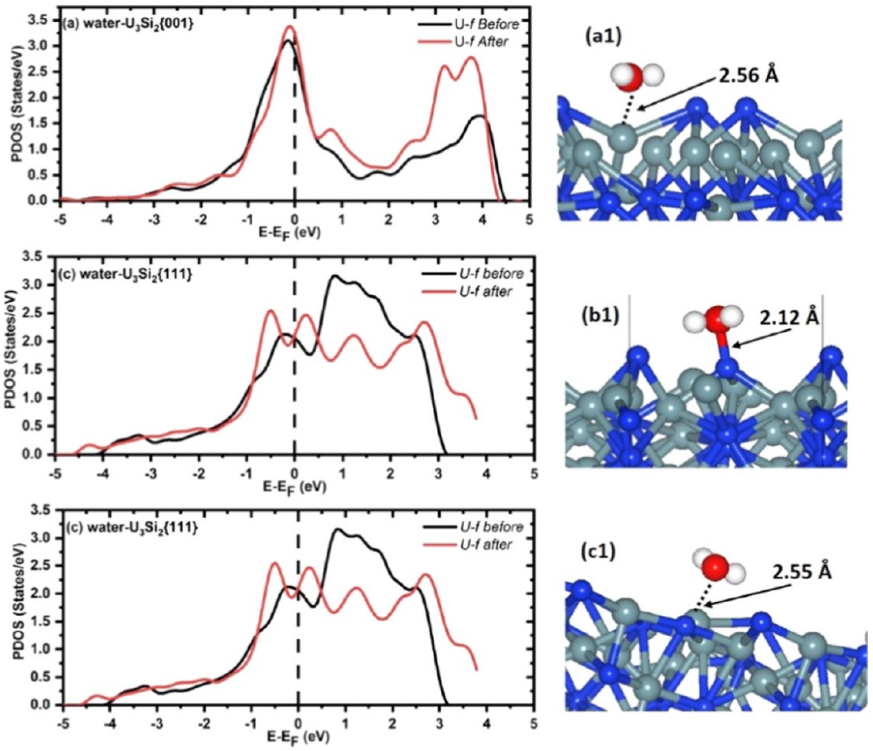

Figure 15. (Right) PDOS for the interacting surface U f-states before and after the adsorption of H_2O at the (a) water−U_3Si_2{001} and (b) for interacting surface Si p-states at the water−U_3Si_2{110} interface, and for the interacting surface U f-states before and after the adsorption of H_2O at the (c) water−U_3Si_2{111} interface. (Left) the corresponding optimized water−U_3Si_2 interfaces with U−O and Si−O bond lengths.

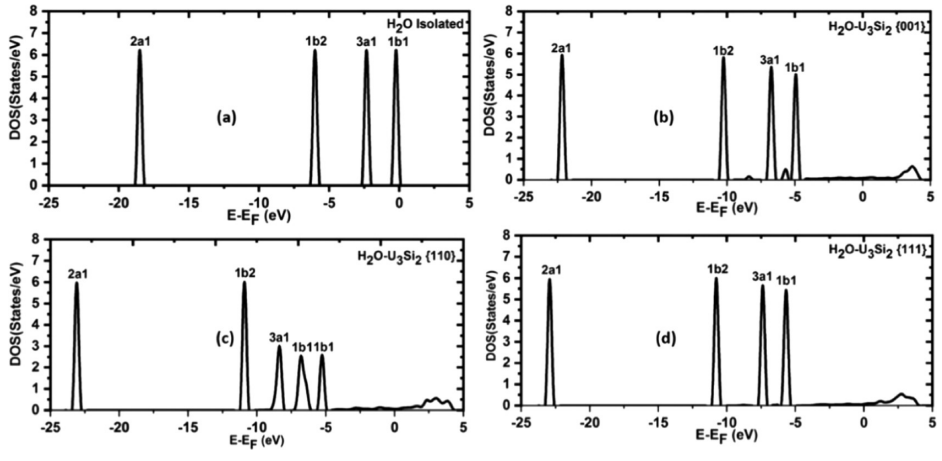

Figure 16. DOS for H_2O in the (a) free state and adsorbed in the lowest-energy geometry at the water−U_3Si_2 interfaces (b−d).

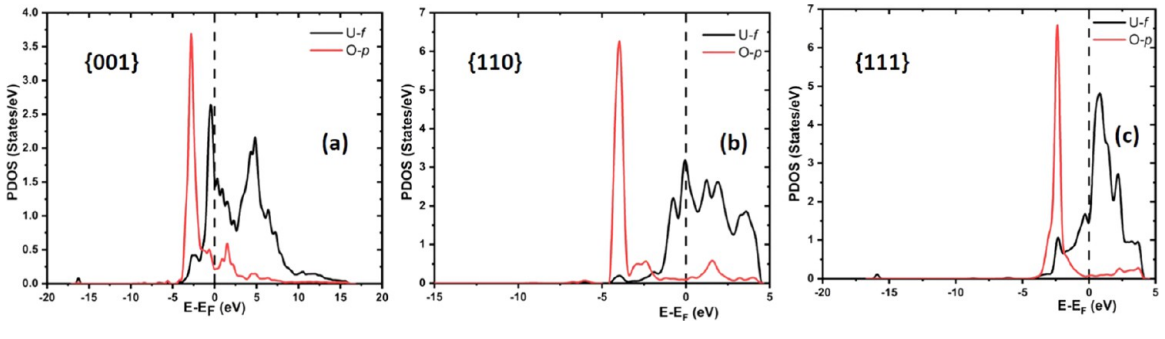

Figure 17. Partial DOS projected on the interacting surface U f-states and O p-states for adsorbed atomic oxygen on the top-U site on (a) {001}, (b) {110}, and (c) {111} surfaces.

DOI: 10.1021/acs.jpcc.9b03076
J. Phys. Chem. C 2019, 123, 19453−19467

electronic states of the surface and oxygen-assisted dissociation of H_2O.

The work function depends on the crystallographic direction as shown by the results in Table 7. The anisotropic nature of the work function comes from the crystallographic arrangement of the surface planes, which determines the spreading of the electronic charge into the vacuum.[54] Furthermore, the adsorption acts to smoothen the surface electric charge distribution that lowers the work function. The work function is such that $\Phi_{(H_2O + O)} < \Phi(_{H_2O}) < \Phi_{dry}$ due to the partial transfer of electron charge from the substrate to the adsorbate and the resulting adsorption-induced surface dipoles (Table 7).[55]

Table 7. Calculated Work Functions of the Dry (Φ_{dry}), Hydrated (Φ_{H_2O}), and Coadsorbed H_2O + O (Φ_{H_2O+O}) U_3Si_2 Surfaces

surface	Φ_{dry} (eV)	Φ_{H_2O} (eV)	Φ_{H_2O+O} (eV)
{001}	3.09	3.05	2.86
{110}	1.89	1.48	1.21
{111}	2.86	2.30	1.96

4. SUMMARY AND CONCLUSIONS

We have investigated the adsorption and dissociation reactions of H_2O on clean, oxygen-covered and defective U_3Si_2{001}, {110}, and {100} surfaces using density functional theory calculations. The adsorption energetics and characteristics of molecular water adsorption were compared with full dissociative and mixed (molecular and dissociative) adsorption modes on the U_3Si_2 surfaces. We showed from our calculations that the major interactions between the adsorbing water molecules and the U_3Si_2 surfaces occur through oxygen and the surface U or Si site. Compared to the clean surfaces, preadsorbed O atoms are shown to enhance the activation of the O−H bonds of water and their subsequent dissociation reactions to form surface hydroxyl species, which are driven by significant charge transfer from the surface to the adsorbing species. We demonstrated that surface vacancy defects enhance the adsorption and dissociation of H_2O compared to a stoichiometric defect-free surfaces. The molecular-level insights derived from this work provide a fundamental understanding of the adsorption processes and mechanisms of the early stage of oxidation of U_3Si_2 in the presence of oxygen and water and might open new avenues for the rational design of oxidation resistance of metallic fuels for nuclear reactors.

ASSOCIATED CONTENT

Supporting Information

The Supporting Information is available free of charge on the ACS Publications website at DOI: 10.1021/acs.jpcc.9b03076.

Mixed mode water adsorption configurations and adsorption energies on stoichiometric U_3Si_2{001}, {110}, and {111} surfaces; calculated adsorption energy (E_{ads}), relevant bond lengths (d) of atomic (O) oxygen on {001}, {110}, and {111} U_3Si_2 surfaces (PDF)

AUTHOR INFORMATION

Corresponding Authors

*E-mail: ericmoore.jossou@usask.ca (E.J.).
*E-mail: jerzy.szpunar@usask.ca (J.S.).

ORCID

Ericmoore Jossou: 0000-0002-4792-760X
Nelson Y. Dzade: 0000-0001-7733-9473

Notes

The authors declare no competing financial interest.

ACKNOWLEDGMENTS

The authors gratefully acknowledge Compute Canada (WestGrid) and University of Saskatchewan's Research Cluster (Plato) for a generous amount of CPU time. We also acknowledge the financial support of the Canadian National Science and Engineering Research Council (NSERC) and the University of Saskatchewan's International Dean's Scholarship. N.Y.D. acknowledges the U.K. Engineering and Physical Sciences Research Council (EPSRC) for funding (Grant No. EP/S001395/1).

REFERENCES

(1) White, J. T.; Nelson, A. T.; Dunwoody, J. T.; Byler, D. D.; Safarik, D. J.; McClellan, K. J. Thermophysical Properties of U_3Si_2 to 1773 K. *J. Nucl. Mater.* **2015**, *464*, 275−280.

(2) Wood, E. S.; White, J. T.; Grote, C. J.; Nelson, A. T. U_3Si_2 Behavior in H_2O: Part I, Fl Owing Steam and the Effect of Hydrogen. *J. Nucl. Mater.* **2018**, *501*, 404−412.

(3) Nelson, A. T.; Migdisov, A.; Wood, E. S.; Grote, C. J. U_3Si_2 Behavior in H_2O Environments: Part II, Pressurized Water with Controlled Redox Chemistry. *J. Nucl. Mater.* **2018**, *500*, 81−91.

(4) Middleburgh, S. C.; Claisse, A.; Andersson, D. A.; Grimes, R. W.; Olsson, P.; Mašková, S. Solution of Hydrogen in Accident Tolerant Fuel Candidate Material: U_3Si_2. *J. Nucl. Mater.* **2018**, *501*, 234−237.

(5) Beeler, B.; Baskes, M.; Andersson, D.; Cooper, M. W. D.; Zhang, Y. A modified Embedded-Atom Method interatomic potential for uranium-silicide. *J. Nucl. Mater.* **2017**, *495*, 267−276.

(6) Noordhoek, M. J.; Besmann, T. M.; Andersson, D.; Middleburgh, S. C.; Chernatynskiy, A. Phase Equilibria in the U-Si System from First-Principles Calculations. *J. Nucl. Mater.* **2016**, *479*, 216−223.

(7) Wang, T.; Qiu, N.; Wen, X.; Tian, Y.; He, J.; Luo, K.; Zha, X.; Zhou, Y.; Huang, Q.; Lang, J.; et al. First-Principles Investigations on the Electronic Structures of U_3Si_2. *J. Nucl. Mater.* **2016**, *469*, 194−199.

(8) Andersson, D. A.; Liu, X.-Y.; Beeler, B.; Middleburgh, S. C.; Claisse, A.; Stanek, C. R. Density Functional Theory Calculations of Self- and Xe Diffusion in U_3Si_2. *J. Nucl. Mater.* **2019**, *515*, 312−325.

(9) Beeler, B.; Baskes, M.; Andersson, D.; Cooper, M. W. D.; Zhang, Y. Molecular Dynamics Investigation of Grain Boundaries and Surfaces in U_3Si_2. *J. Nucl. Mater.* **2019**, *514*, 290−298.

(10) Middleburgh, S. C.; Grimes, R. W.; Lahoda, E. J.; Stanek, C. R.; Andersson, D. A. Non-Stoichiometry in U_3Si_2. *J. Nucl. Mater.* **2016**, *482*, 300−305.

(11) Remschnig, K.; Le Bihan, T.; Noël, H.; Rogl, P. Structural Chemistry and Magnetic Behavior of Binary Uranium Silicides. *J. Solid State Chem.* **1992**, *97*, 391−399.

(12) Bo, T.; Lan, J.; Zhao, Y.; Zhang, Y.; He, C.; Chai, Z.; Shi, W. Surface Science Surface Properties of NpO_2 and Water Reacting with Stoichiometric and Atomistic Thermodynamics. *Surf. Sci.* **2016**, *644*, 153−164.

(13) Bo, T.; Lan, J.-H.; Zhao, Y.-L.; Zhang, Y.-J.; He, C.-H.; Chai, Z.-F.; Shi, W.-Q. Surface Properties of NpO_2 and Water Reacting with Stoichiometric and Reduced NpO_2 (111), (110), and (100) Surfaces from *Ab Initio* Atomistic Thermodynamics. *Surf. Sci.* **2016**, *644*, 153−164.

DOI: 10.1021/acs.jpcc.9b03076
J. Phys. Chem. C 2019, 123, 19453−19467

(14) Jossou, E.; Eduok, U.; Dzade, N. Y.; Szpunar, B.; Szpunar, J. A. Oxidation Behaviour of U_3Si_2: An Experimental and First Principles Investigation. *Phys. Chem. Chem. Phys.* **2018**, *20*, 4708−4720.
(15) Molinari, M.; Parker, S. C.; Sayle, D. C.; Islam, M. S. Water Adsorption and Its Effect on the Stability of Low Index Stoichiometric and Reduced Surfaces of Ceria. *J. Phys. Chem. C* **2012**, *116*, 7073−7083.
(16) Bo, T.; Lan, J.-H.; Wang, C.-Z.; Zhao, Y.-L.; He, C.-H.; Zhang, Y.-J.; Chai, Z.-F.; Shi, W.-Q. First-Principles Study of Water Reaction and H2 Formation on UO_2 (111) and (110) Single Crystal Surfaces. *J. Phys. Chem. C* **2014**, *118*, 21935−21944.
(17) Fan, J.; Li, C.; Zhao, J.; Shan, Y.; Xu, H. The Enhancement of Surface Reactivity on CeO_2 (111) Mediated by Subsurface Oxygen Vacancies. *J. Phys. Chem. C* **2016**, *120*, 27917−27924.
(18) Zhukovskii, Y.; Bocharov, D.; Gryaznov, D.; Kotomin, E. *First Principles Simulations on Surface Properties and Oxidation of Nitride Nuclear Fuels*; Advances in Nuclear Fuel; IntechOpen, 2012.
(19) Wellington, J. P. W.; Tegner, B. E.; Collard, J.; Kerridge, A.; Kaltsoyannis, N. Oxygen Vacancy Formation and Water Adsorption on Reduced AnO_2{111}, {110}, and {100} Surfaces (An = U, Pu): A Computational Study. *J. Phys. Chem. C* **2018**, *122*, 7149−7165.
(20) Hohenberg, P.; Kohn, W. Inhomogeneous Electron Gas. *Phys. Rev.* **1964**, *136*, B864−B871.
(21) Kohn, W.; Sham, L. J. Self-Consistent Equations Including Exchange and Correlation Effects. *Phys. Rev.* **1965**, *140*, A1133−A1138.
(22) Giannozzi, P.; Baroni, S.; Bonini, N.; Calandra, M.; Car, R.; Cavazzoni, C.; Ceresoli, D.; Chiarotti, G. L.; Cococcioni, M.; Dabo, I.; et al. QUANTUM ESPRESSO: A Modular and Open-Source Software Project for Quantum Simulations of Materials. *J. Phys.: Condens. Matter* **2009**, *21*, No. 395502.
(23) Wu, Z.; Cohen, R. E. More Accurate Generalized Gradient Approximation for Solids. *Phys. Rev. B* **2006**, *73*, No. 235116.
(24) Liechtenstein, A. I.; Anisimov, V. I.; Zaanen, J. Density-Functional Theory and Strong Interactions: Orbital Ordering in Mott-Hubbard Insulators. *Phys. Rev. B* **1995**, *52*, R5467−R5470.
(25) Methfessel, M.; Paxton, A. T. High-Precision Sampling for Brillouin-Zone Integration in Metals. *Phys. Rev. B* **1989**, *40*, 3616−3621.
(26) Head, J. D.; Zerner, M. C. A Broyden—Fletcher—Goldfarb—Shanno Optimization Procedure for Molecular Geometries. *Chem. Phys. Lett.* **1985**, *122*, 264−270.
(27) Momma, K.; Izumi, F. VESTA: A Three-Dimensional Visualization System for Electronic and Structural Analysis. *J. Appl. Crystallogr.* **2008**, *41*, 653−658.
(28) Momma, K.; Izumi, F. VESTA3 for Three-Dimensional Visualization of Crystal, Volumetric and Morphology Data. *J. Appl. Crystallogr.* **2011**, *44*, 1272−1276.
(29) Watson, G. W.; Kelsey, E. T.; de Leeuw, N. H.; Harris, D. J.; Parker, S. C. Atomistic Simulation of Dislocations, Surfaces and Interfaces in MgO. *J. Chem. Soc., Faraday Trans.* **1996**, *92*, 433−438.
(30) Bader, R. F. W. Atoms in Molecules. *Acc. Chem. Res.* **1985**, *18*, 9−15.
(31) Andersson, A. D. *Density Functional Theory Calculations of Defect and Fission Gas Properties in U-Si Fuels*; Office of Scientific and Technical Information, 2016.
(32) Li, R.; Zhang, P.; Zhang, C.; Huang, X.; Zhao, J. Vacancy Trapping Mechanism for Multiple Helium in Monovacancy and Small Void of Vanadium Solid. *J. Nucl. Mater.* **2013**, *440*, 557−561.
(33) Lide, D. R. *Handbook of Chemistry and Physics*, 82nd ed.; CRC Press: Boca Raton, FL, 2001.
(34) Dzade, N. Y.; Roldan, A.; de Leeuw, N. H. DFT-D2 Study of the Adsorption and Dissociation of Water on Clean and Oxygen-Covered {001} and {011} Surfaces of Mackinawite (FeS). *J. Phys. Chem. C* **2016**, *120*, 21441−21450.
(35) Herzberg, G. *Molecular Spectra and Molecular Structure. II. Infrared and Raman Spectra of Polyatomic Molecules*; Lancaster Press: New York, 1946; p 365.
(36) Bo, T.; Lan, J.; Zhang, Y.; Zhao, Y.; He, C.; Chai, Z.; Shi, W. Surface of Uranium Mononitride: Energetics And. *Phys. Chem. Chem. Phys.* **2016**, *18*, 13255−13266.
(37) Bo, T.; Lan, J.; Zhao, Y.; Zhang, Y.; He, C.; Chai, Z.; Shi, W. First-Principles Study of Water Adsorption and Dissociation on the UO_2. *J. Nucl. Mater.* **2014**, *454*, 446−454.
(38) Shapovalov, V.; Truong, T. N. Ab Initio Study of Water Adsorption on α-Al_2O_3 (0001) Crystal Surface. *J. Phys. Chem. B* **2000**, *104*, 9859−9863.
(39) Pang, Z.; Duerrbeck, S.; Kha, C.; Bertel, E.; Somorjai, G. A.; Salmeron, M. Adsorption and Reactions of Water on Oxygen-Precovered Cu(110). *J. Phys. Chem. C* **2016**, *120*, 9218−9222.
(40) Chen, L.; Lu, J.; Liu, P.; Gao, L.; Liu, Y.; Xiong, F.; Qiu, S.; Qiu, X.; Guo, Y.; Chen, X. Dissociation and Charge Transfer of H_2O on Cu(110) Probed in Real Time Using Ion Scattering Spectroscopy. *Langmuir* **2016**, *32*, 12047−12055.
(41) Taylor, C. D.; Lookman, T.; Lillard, R. S. *Ab Initio* Calculations of the Uranium−Hydrogen System: Thermodynamics, Hydrogen Saturation of a -U and Phase-Transformation to UH_3. *Acta Mater.* **2010**, *58*, 1045−1055.
(42) Bo, T.; Lan, J.-H.; Zhang, Y.-J.; Zhao, Y.-L.; He, C.-H.; Chai, Z.-F.; Shi, W.-Q. Adsorption and Dissociation of H_2O on the (001) Surface of Uranium Mononitride: Energetics and Mechanism from First-Principles Investigation. *Phys. Chem. Chem. Phys.* **2016**, *18*, 13255−13266.
(43) Tian, X.; Wang, H.; Xiao, H.; Gao, T. Adsorption of Water on UO_2 (111) Surface: Density Functional Theory Calculations. *Comput. Mater. Sci.* **2014**, *91*, 364−371.
(44) Tegner, B. E.; Molinari, M.; Kerridge, A.; Parker, S. C.; Kaltsoyannis, N. Water Adsorption on AnO_2 {111}, {110}, and {100} Surfaces (An = U and Pu): A Density Functional Theory + U Study. *J. Phys. Chem. C* **2017**, *121*, 1675−1682.
(45) Schoenes, J. Optical Properties and Electronic Structure of UO_2. *J. Appl. Phys.* **1978**, *49*, 1463−1465.
(46) Wang, J.; Ewing, R. C.; Becker, U. Electronic Structure and Stability of Hyperstoichiometric UO_{2+x} under Pressure. *Phys. Rev. B* **2013**, *88*, No. 024109.
(47) Henderson, M. A. The Interaction of Water with Solid Surfaces: Fundamental Aspects Revisited. *Surf. Sci. Rep.* **2002**, *46*, 1−308.
(48) Ammon, C.; Bayer, A.; Steinrück, H.-P.; Held, G. Low-Temperature Partial Dissociation of Water on Cu(110). *Chem. Phys. Lett.* **2003**, *377*, 163−169.
(49) Jiang, Z.; Fang, T. Dissociation Mechanism of H_2O on Clean and Oxygen-Covered Cu(111) Surfaces: A Theoretical Study. *Vaccum* **2016**, *128*, 252−258.
(50) Johnson, K.; Ström, V.; Wallenius, J.; Lopes, D. A. Oxidation of Accident Tolerant Fuel Candidates. *J. Nucl. Sci. Technol.* **2017**, *54*, 280−286.
(51) Johnson, K. D.; Wallenius, J.; Jolkkonen, M.; Claisse, A. Spark Plasma Sintering and Porosity Studies of Uranium Nitride. *J. Nucl. Mater.* **2016**, *473*, 13−17.
(52) Li, J.; Zhu, S.; Li, H.; Oguzie, E. E.; Li, Y.; Wang, F. Bonding Nature of Monomeric H_2O on Pd: Orbital Cooperation and Competition. *J. Phys. Chem. C* **2009**, 1931−1938.
(53) Akbay, T.; Staykov, A.; Druce, J.; Téllez, H.; Ishihara, T.; Kilner, J. A. The interaction of molecular oxygen on LaO terminated surfaces of La_2NiO_4. *J. Mater. Chem. A* **2016**, *4*, 13113.
(54) Fall, C. *Ab Initio Study of the Work Functions of Elemental Metal Crystals*; EPFL PP: Lausanne.
(55) Zhang, W.; Liu, L.; Wan, L.; Liu, L.; Cao, L.; Xu, F.; Zhao, J.; Wu, Z. Electronic Structures of Bare and Terephthalic Acid Adsorbed TiO_2(110)-(1 × 2) Reconstructed Surfaces: Origin and Reactivity of the Band Gap States. *Phys. Chem. Chem. Phys.* **2015**, *17*, 20144−20153.

DOI: 10.1021/acs.jpcc.9b03076
J. Phys. Chem. C 2019, 123, 19453−19467